========== **PROCEEDINGS OF THE III INTERNATIONAL CONFERENCE** ========
========== **"MATHEMATICAL BIOLOGY AND BIOINFORMATICS"**==========

Electronic Structure of the Active Site of Truncated Hemoglobin N in MCSCF Approach

Simon K.V. and Tulub A.V.[*]

Saint-Petersburg State University

Abstract. The MCSCF approach with the geometry optimization is applied to the calculation of electronic properties of active site of heme trHbN including (ONOO) functional group and two water molecules. The localized molecular orbitals are employed as a starting set. Two subspaces of full interaction (CAS) have been used by the construction of MCSCF wavefunction, the first one includes 3d-orbitals of iron atom and the second contains bonding and antibonding molecular orbitals (MOs) of peroxynitrite with one unshared electronic pair of the O_2 fragment. The geometry of the anionic $(ONOO)^-$ structures arising due to the charge transfer from Fe(II) are close to that of nitrate anion and peroxynitrite in gas phase. The peroxynitrite is considered in its turn in two different forms corresponding to singlet and triplet states of this anion in the gas phase. The possible role of peroxynitrite structure is discussed in a connection with the defense reaction of *M. tuberculosis*.

Key words: *tubercular bacillus defense reaction, electronic structure of heme active center, multiconfiguration self-consistent field (MCSCF) wavefunctions*.

INTRODUCTION

Truncated hemoglobin N (trHbN), a member of a hemoprotein family, is an integral part of the tubercular bacillus hemoglobin, *M. tuberculosis*. Recent years show an increasing interest to the trHbN structure, especially with the finding of the bacillus' defense reaction, which, thanks to macrophages, produces NO radical as an immune system response to infection. We summarize below in a brief mode some known structure properties of trHbN.

The trHbN reveals two channels – a long (20Å) and a short (8Å) – through which the diffusion of NO and O_2 occurs to the heme core – a ferroprotoporphyrin containing ring (FeP) [1, 2]. The diffusion is highly dependent on the activation barriers studied earlier by the MD methods [3, 4]. When the *M. tuberculosis* is in a latent state, the active heme site produces the nitrate ion according to reaction (1):

$$NO + O_2 + Fe(II) \rightarrow NO_3^- + Fe(III). \tag{1}$$

The NO_3^- diffusion in the heme occurs through the third channel. With the Fe-NO_3 length increase, the diffusion is mostly regulated by interaction with the amino acid fragments, GlnE and TyrB, to which the NO_3^- anion is bound through hydrogen bonding [5, 6]. The process ends in removing the NO_3^-.

The initial stage of the process, which starts by breaking the bond with Fe, is highly sensitive to interaction of the NO_3^- with water molecules. In the gaseous phase the formation of NO_3^- from O_2^- and NO radical does not occur. Instead of the nitrate anion NO_3^- the peroxynitrite $(ONOO)^-$ is produced via reaction (2):

---

[*] tulub@nk7099.spb.edu

$$NO + O_2^- = (ONOO)^-. \tag{2}$$

The peroxynitrite is of high interest in biochemistry as a strong oxidizer along with other famous oxidants like O_2^-, OH^- and H_2O_2. Quantum chemistry computations reveal fine electronic structure and geometry of the isolated $(ONOO)^-$ along with its complexes with water. The calculation of electronic characteristics of peroxynitrite anion needs a detailed accounting for electronic correlation energy [6–8]. The ground state of NO_3^- has a symmetry of a regular triangle D_{3h}, the $(ONOO)^- \rightarrow NO_3^-$ regrouping is unfavorable due to remarkable activation barriers [9].

Electronic properties of the active heme core strongly correlate with conformational changes of the protein and the amino acid environment, the latter is of major impact on reaction (1). A key problem is in finding a way of how *M. tuberculosis* to be recovered from a latent state. One might assume that the cavity in the heme around the active core remains unchanged. Small perturbations in the hole structure might be significant only at the latest stage of the process, and these changes might affect the reaction profile between the NO and O_2^- in the FeP. Additionally, the reaction profile is highly sensitive to the presence of other possible structures arising upon interaction with the nitrogen oxide.

We consider the following reaction channel:

$$NO + O_2 + Fe(II) \rightarrow (ONOO)^- + Fe(III), \tag{3}$$

the peroxynitrite formation is assumed to occur in its ground state as well in the dimeric form [9].

The whole complex includes iron ferroporphyrin (FeP), imidazole ($C_3N_2H_4$), two water molecules connected to NO_3^- or $(ONOO)^-$ anions. The latter anions appear as a result of charge transfer from FeP onto (ONOO) fragment, the whole electronic structure is represented bellow.

Consider first the approach of NO^- anion (ground state $^3\Sigma^-$) and O_2 ($^3\Sigma_g^-$), the total spin takes the values S = 2,1,0. The S = 2 state is unstable [9], the triplet state can be considered as the dimeric form of peroxynitrite. The almost exact coincidence of total energies of singlet and triplet states takes place in the vicinity of local minimum of $(ON\cdots OO)^-$ anion in a gas phase [9]. This fact facilitates the spin change in the course of a reaction, such processes arise much interest at the recent time, see the review articles [12–14].

The various versions of multiconfiguration self-consistent field (MCSCF) method were used earlier treating different spin states of $(ONOO)^-$ [9], we follow below the same approach. The wave function of the system is intended to be the exact eigenfunction of S^2 operator. The numerical results are presented in the order: 1) choice of iron atom basis set, 2) calculation of ground and first low-lying excited states of FeP, 3) description of peroxynitrite and nitrate anion structures in molecular complex which includes also two water molecules.

ELECTRONIC STRUCTURE OF FeP AND PEROXYNITRITE

The calculations were performed by means of GAMESS (2009) program [15], the MCSCF method was employed on the ground of restricted CI expansions [16]. The system is characterized by a substantial charge transfer from iron porphyrin ring onto $[(O_2NO)(H_2O)_2]$ complex, the main role is due to iron atom which acquires an additional positive charge. The ionization potentials (IP) of iron, that is (IP1) (IP2) and (IP3) are substantially dependent on chosen basis set and calculation scheme. This may lead to appreciable difference in the second or in the third ionization potential, while obtaining a good value for the first one, sometimes arise the reverse situation. A special basis set was chosen for iron atom, it includes functions from 6-31G(f) basis set for Fe with three supplementary Gaussian s-, p- and d-shells added. The exponents of this added shells were optimized keeping the original functions of 6-31G* basis set unchangeable. Various methods such as ROMP2, MCQDPT [17] and

24

coupled cluster CR-CC(2, 3) [18, 19] yield closer values of exponents after optimization of total energy of ground state of iron atom (the ^5D term). The values obtained on the CR-CC(2, 3) level are:

$$\zeta(s)=0.280829, \zeta(p)=0.120767, \zeta(d)=0.136335.$$

This basis set, denoted as 6-31G*(s, p, d), was used to obtain first ionization potentials (as differences of total energy) of iron atom in ROMP2 and CR-CC(2, 3) methods, the values are presented in Table 1. It is interesting to note, that relativistic method HFD (numerical integration of HFD equations) reproduces ionization potentials quite reasonable: IP1 = 6.88eV, IP2 = 16.18eV and IP3 = 31.71eV.

Table 1. Total energies and ionization potentials of Fe atom in ROMP2 and CR-CC(2, 3) methods with 6-31G*(s, p, d) basis set

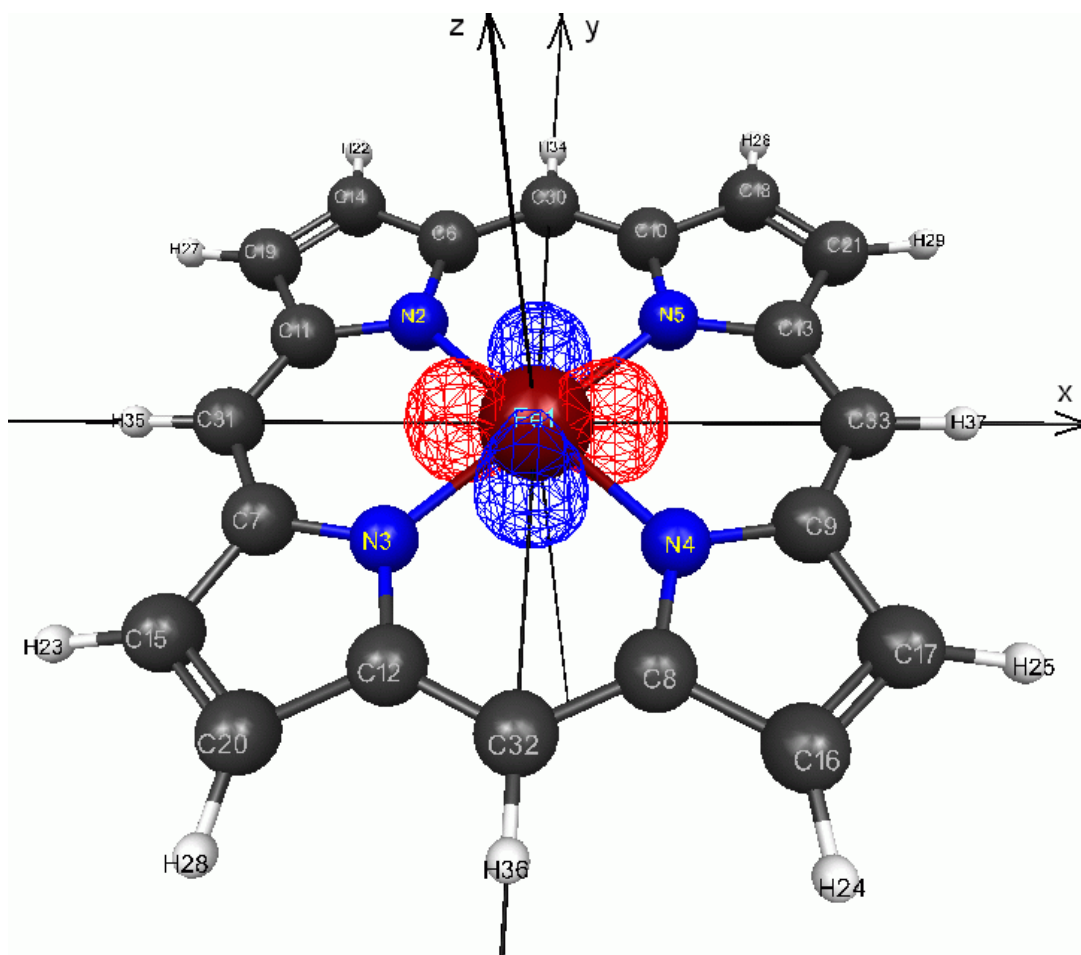| Charge	Term	ROMP2		CR-CC(2,3)		Exp. IP, eV
		E, a.u.	IP, eV	E, a.u.	IP, eV	
Fe^0	^5D_g	−1262.604250	7.427	−1262.627364	7.715	7.896
Fe^+	^6D_g	−1262.331313	15.96	−1262.343845	16.02	16.18
Fe^{2+}	^5D_g	−1261.744718	30.26	−1261.755008	30.08	30.64
Fe^{3+}	^6S_g	−1260.632847	—	−1260.649719	—	—

Figure 1. Iron porphyrin molecule and the active $3d(x^2\text{-}y^2)$ orbital of iron atom.

Consider next the optimal geometry and the lowest excited states energies of FeP, atomic numeration is given in Figure 1. The subspace of full interaction for RASSCF method [16] was set to include the orbitals of 3d-shell of iron atom, two occupied and two virtual orbitals

25

of porphyrin ring were used as "lower" and "upper" subspaces respectively, see Table 1 in Appendix 1. The maximum excitation level between subspaces equals two. The 4s-electrons are delocalized in the plain of porphyrin ring forming coordination bonds. The used basis sets are given in Table 3 of Appendix 1.

The ground term of plain D_{4h} symmetry FeP ring is $^5A_{1g}$, geometry is represented on Figure 1 and optimized Fe-N bond lengths in Table 2 in Appendix 1. The atomic charges in Mulliken scheme are given in Table 3 in the same Appendix. The 3d wavefunctions are closely localized near iron atom and the charge of iron atom equals +1.69 units of elementary charge. The charges of nitrogen atoms holding the central iron atom are close to -1.30. Such significant negative charges facilitate additional stabilization of iron cation in porphyrin ring. The wavefunction of $^5A_{1g}$ state is qualitatively well described by Hartree-Fock method with doubly occupied $(3z^2-r^2)$ orbital in 3d-shell of iron atom (Table 1 in Appendix 1).

The energies of the lowest excited states evaluated in optimal geometry of the ground $^5A_{1g}$ state are given in Table 2, they were calculated by means of RASCI method with the same choice of active space (Table 1 in Appendix1). The molecular orbitals for RASCI method were obtained using RASSCF calculation with MO optimization for group of 8 lowest states. This is the cause of change of the total energy of $^5A_{1g}$ term in the Table 2 from that in the Table 2 of Appendix 1.

Table 2. The lowest electronic states of iron porphyrin molecule evaluated at the optimal geometry of the ground $^5A_{1g}$ state (the RASCI method)

№	Term	Total energy, a.u.	Relative energy, eV	Dominating configurations in 3d-shell
0	$^5A_{1g}$	−2244.251999	0	$(15a_{1g})^2(9b_{1g})^1(4e_g)^2(10b_{2g})^1$ $C^2=0.94$
1	^5E_g	−2244.245381	0.180	$(15a_{1g})^1(9b_{1g})^1(4e_g)^3(10b_{2g})^1$ $C^2=0.94$
2	$^5B_{1g}$	−2244.236585	0.419	$(15a_{1g})^1(9b_{1g})^2(4e_g)^2(10b_{2g})^1$ $C^2=0.94$
3	$^3A_{2g}$	−2244.203736	1.313	$(15a_{1g})^2(9b_{1g})^2(4e_g)^2(10b_{2g})^0$ $C^2=0.89$
4	^3E_g	−2244.202493	1.347	$(15a_{1g})^1(9b_{1g})^2(4e_g)^3(10b_{2g})^0$ $C^2=0.79$ $(15a_{1g})^2(9b_{1g})^1(4e_g)^3(10b_{2g})^0$ $C^2=0.11$
5	$^3B_{1g}$	−2244.184790	1.829	$(15a_{1g})^1(9b_{1g})^1(4e_g)^4(10b_{2g})^0$ $C^2=0.78$ $(15a_{1g})^1(9b_{1g})^2(4e_g)^2(10b_{2g})^1$ $C^2=0.13$
6	$^5B_{2g}$	−2244.166340	2.331	$(15a_{1g})^1(9b_{1g})^1(4e_g)^2(10b_{2g})^2$ $C^2=0.94$
7	^3E_g	−2244.163050	2.420	$(15a_{1g})^2(9b_{1g})^1(4e_g)^3(10b_{2g})^0$ $C^2=0.42$ $(15a_{1g})^1(9b_{1g})^1(4e_g)^3(10b_{2g})^1$ $C^2=0.30$ $(15a_{1g})^2(9b_{1g})^2(4e_g)^1(10b_{2g})^1$ $C^2=0.13$
8	$^1A_{1g}$	−2244.155102	2.637	$(15a_{1g})^0(9b_{1g})^2(4e_g)^4(10b_{2g})^0$ $C^2=0.79$ $(15a_{1g})^2(9b_{1g})^2(4e_g)^2(10b_{2g})^0$ $C^2=0.10$ $(15a_{1g})^2(9b_{1g})^0(4e_g)^4(10b_{2g})^0$ $C^2=0.02$

The lowest excited state of iron porphyrin molecule is the ^5E_g state with excitation energy near 0.18eV. The excitation energy of the lowest triplet state $^3A_{2g}$ is 1.31eV and of the lowest singlet state $^1A_{1g}$ is 2.64eV. This both states are also qualitatively well described by Hartree-Fock configurations, see the dominating configurations. Among the given 8 excited states excitation energies which are below 2.64eV there are no states with substantial contributions from porphyrin ring excitations, all excitations are mainly due to various spin states of iron 3d-shell.
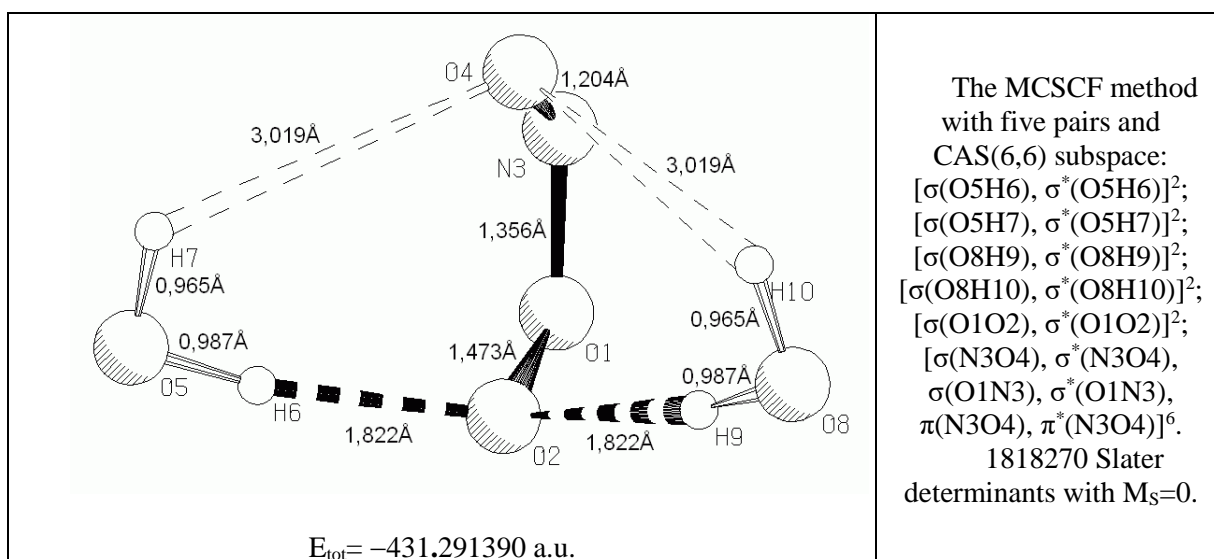
The characteristics of the lowest triplet $^3A_{2g}$ and singlet $^1A_{1g}$ states in their own optimal geometry are given in Table 2 in Appendix 1. The geometry optimization slightly lowers their energies relative to the ground state: 1.21eV for the triplet state and 2.52eV for the singlet one. For the $^1A_{1g}$ state the broken symmetry solution was obtained: the symmetry reduced to C_S. The total energy of the same solution with symmetry restrictions of D_{4h} group is only 7×10^{-6}a.u. higher than the energy given in the Table 2 of Appendix 1. The $^1A_{1g}$ term is not a

26

degenerate one and this small lowering in energy is in the range of error of the method used, it may be due to the non optimal choice of active space for this state. This solution causes differences in bond lengths in fourth digit after decimal point, the averaged Fe-N bond length is given. The $^1B_{2g}$ term is not described by single Slater determinant, its total energy in optimized geometry is only 0.16eV higher than that for $^1A_{1g}$ term. Very small differences are noticeable in Mulliken charges of equivalent atoms in the case of $^1A_{1g}$ state, their origin is due to the symmetry breaking, Table 3 in Appendix 1 contains the averaged values.

One can conclude from the above listed data, that ground state of the plain FeP molecule is a quintet state. Imidazole molecule does not change the total spin of a system, but it may cause possible shift of an iron atom relative to ring plain. The optimization of a whole system is done below, therefore the effect of an imidazole on position of iron atom is not considered separately. The typical coordination number of iron atom equals six and the formation of two additional bonds takes place. The fifth bond forms with nitrogen atom in imidazole and the sixth one with oxygen molecule, this bond is accompanied by electron transfer from 3d-shell of an iron atom onto O_2 fragment. When (ONOO) radical is attached to FeP with ground state spin number $S = 2$, the total spin will be $S = 5/2$ or $S = 3/2$. According to the Hund rule the total spin is accepted to be $S = 5/2$ and in the case of dimeric structure of a peroxynitrite the total spin is set to $S = 7/2$.

Consider now $[O_2+NO]^- + 2(H_2O)$ complex structure, first in gas phase. It is represented in the figure of Table 3, all numerical data are given in the basis of localized MOs in MCSCF approach according to [9]. The peroxynitrite structure seems to be caught almost in pincers between two water molecules.

Table 3. The structure of $[O_2+NO]^- + 2(H_2O)$ complex in the MCSCF method

The MCSCF method with five pairs and CAS(6,6) subspace:
$[\sigma(O5H6), \sigma^*(O5H6)]^2$;
$[\sigma(O5H7), \sigma^*(O5H7)]^2$;
$[\sigma(O8H9), \sigma^*(O8H9)]^2$;
$[\sigma(O8H10), \sigma^*(O8H10)]^2$;
$[\sigma(O1O2), \sigma^*(O1O2)]^2$;
$[\sigma(N3O4), \sigma^*(N3O4), \sigma(O1N3), \sigma^*(O1N3), \pi(N3O4), \pi^*(N3O4)]^6$.
1818270 Slater determinants with $M_S=0$.

$E_{tot}= -431.291390$ a.u.

ELECTRONIC STRUCTURE OF TOTAL COMPLEX

We consider the arrangement of atoms corresponding to peroxynitrite and nitrate anion structures in the framework of the whole molecular system. The "Aufbau" of MCSCF wavefunction is similar to that in the Table 3, the technique of MO visualization can be found in [20]. The calculation routine steps are described below.

At the first step the UHF molecular wave function was found for the total spin $S = 2.5$ with maximum possible spin projection $Ms = 2.5$, that implies assignment of total numbers of electrons with spin "up" (α) and "down" (β). The natural orbitals (NOs) of UHF method were generated and the nine of them with the occupation numbers close to 1 were selected. These NOs were examined by means of MacMolPlt [20] or Chemcraft program and they were only partially localized on 3d-functions of iron atom. After that the standard CASSCF method was

27

employed.

As the starting set for active orbitals the 9 UHF NOs with occupations close to 1 were assigned and then calculation for wavefunction with total spin S = 2.5 was performed by means of SOSCF optimization routine. After 100 iterations NOs in CASSCF method were obtained and again examined: 7 of them had occupations close to 1 and also were only partially localized in 3d-shell of iron atom. These 7 natural orbitals were further optimized (SOSCF optimizer) in the frame of MCSCF method including single configuration for total spin S = 3.5. Among the obtained 7 active orbitals 2 had the shapes resembling the π-orbitals of NO fragment in peroxynitrite, they describe the excitation of π→π* type for N3-O4 π-bond. This two orbitals were removed from the active space (the first as the core orbital and the second as the virtual one) and the remaining 5 orbitals most of all resembling the 3d-functions of iron atom were again optimized by means of MCSCF with single configuration with S = 2.5 using SOSCF optimizer. The obtained in such way active singly occupied orbitals most of all resemble the localized and obtained above 3d-functions for iron atom in FeP ring. This solution corresponds to ROHF solution for S = 2.5 with the same total energy.
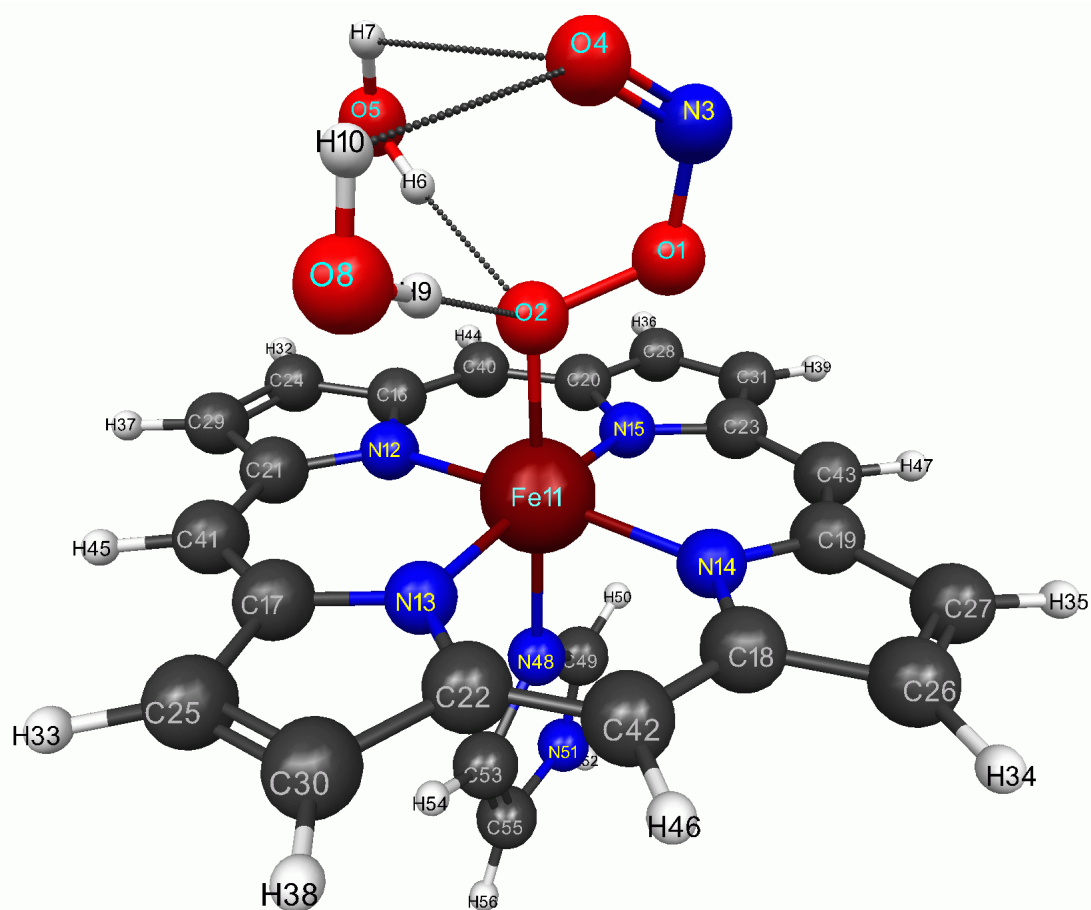

Figure 2. The optimal geometry of complex $[(H_2O)_2OO-NO]$ + Fe-porphyrin + imidazole.

Here we emphasize, that ROHF calculation gives possibility to obtain the Boys localized occupied orbitals (LOCAL=BOYS) and the modified virtual orbitals (MVOQ= -1 algorithm), which resemble antibonding molecular orbitals (MOs) for valence bonds in a molecule. In this case virtual MOs are obtained by diagonalizing the Fock operator of a very positive ion, within the virtual orbital space only, so as each occupied orbital is half filled. The localized and the modified virtual MOs were again examined by means of mentioned visualization programs and only those of them were taken into account, which resembled most of all the

28

necessary bonding and antibonding MOs for valence bonds in peroxynitrite, the singly occupied 3d-orbitals of iron atom were taken unchanged.

The obtained localized MOs were used as the starting set for MCSCF calculation with geometry optimization of whole structure. Two subspaces of full interaction (CAS) were assigned in the MCSCF wavefunction: the first subspace included 3d-orbitals of an iron atom and the second one included 4 pairs of molecular orbitals (bonding and antibonding) describing the chemical bonds in peroxynitrite with one additional orbital of unshared electronic pair on O_2 fragment. The shapes of some active molecular orbitals are represented in Appendix 2. The multiconfiguration task was treated using the ORMAS algorithm [21], the following occupation restrictions for subspaces were assigned:

subspace 1 [3d] 6(max) – 5(min) electrons;
subspace 2 [φ(O1), σ(N3O4), σ(O1N3), σ(O1O2), π(N3O4),
π*(N3O4), σ*(O1O2), σ*(O1N3), σ*(N3O4)] 10(max) – 9(min) electrons.

Such restrictions on occupancies ensure the possibility of electron transfer from 3d-shell of an iron atom onto peroxynitrite. The designed wavefunction belongs to ^6A term with quantum number $S = 2.5$. The optimal geometry of complex $[(H_2O)_2OO\text{-}NO] + Fe$-porphyrin + imidazole including anion $[O_2+NO]^-$ with peroxynitrite structure is given in Figure 2.

The total energy of ^6A term in the used basis set (488 Gaussian basis functions) equals -2900.03020a.u., the geometry optimization is performed with accuracy up to 10^{-4}a.u. for maximum gradient. The Hartree-Fock configuration is of the main importance in the obtained hextet wavefunction, it has the weight $C^2 = 0.80$, the singly occupied orbitals being 3d-shell functions of an iron atom. The unpaired electrons persist in 3d-shell of an iron atom in the configurations corresponding to occupation of antibonding orbitals in peroxynitrite.

The configuration corresponding to the reverse charge transfer from peroxynitrite into 3d-shell of iron atom contributes with negligible weight $C^2 = 0.003$, the doubly occupied being the 3d-shell orbital shown in the Figure 1 in Appendix 2. One can understand the Fe(III) as being described by such type of wavefunction, which agrees well with Mulliken charge +2.84 of iron atom, the Table 4 contains charges of all atoms along with the basis sets used. It is worth to note the substantial negative charges of nitrogen atoms N12, N13, N14 and N15, such redistribution of charge facilitates the stabilization of iron atom in porphyrin ring.

Some characteristics of a peroxynitrite fragment hydrated by two water molecules can be compared now in the gas phase and in the active center of hemoglobin, the data are collected in the Table 5. The peroxide bond length O1-O2 becomes noticeably longer after hydrotation of a peroxynitrite and the r(O1N3) distance noticeably decreases being hydrated by two water molecules in the active center of hemoglobin (Figure 2). These changes may be interpreted from the chemical point of view as the weakening of a peroxide bond O1-O2 and the stabilization of a NO_2 fragment. This should point indirectly on the lowering of activation energy in the reaction of a peroxynitrite rearrangement into the nitrate anion, which is accomplished by the isolation of NO_2 fragment in the transition state point. The activation energy of this reaction in gas phase is approximately 36.2kcal/mol [9].

Table 4. The Mulliken charges of atoms and the basis sets used

Atom	Charge	Basis set	Atom	Charge	Basis set
O1	−0.356	aug-cc-pVDZ	C29	−0.147	6-31G
O2	−0.758	aug-cc-pVDZ	C30	−0.091	6-31G
N3	0.725	aug-cc-pVDZ	C31	−0.151	6-31G
O4	−0.579	aug-cc-pVDZ	H32	0.090	STO-6G
O5	−0.763	6-31G++(d,p)	H33	0.091	STO-6G

29

H6	0.430	6-31G++(d,p)	H34	0.090	STO-6G	
H7	0.357	6-31G++(d,p)	H35	0.089	STO-6G	
O8	−0.754	6-31G++(d,p)	H36	0.088	STO-6G	
H9	0.416	6-31G++(d,p)	H37	0.090	STO-6G	
H10	0.360	6-31G++(d,p)	H38	0.091	STO-6G	
Fe11	2.840	6-31G*(s,p,d)	H39	0.087	STO-6G	
N12	−1.191	6-31G	C40	−0.108	6-31G	
N13	−1.248	6-31G	C41	−0.195	6-31G	
N14	−1.180	6-31G	C42	−0.189	6-31G	
N15	−1.184	6-31G	C43	−0.107	6-31G	
C16	0.402	6-31G	H44	0.087	STO-6G	
C17	0.470	6-31G	H45	0.087	STO-6G	
C18	0.465	6-31G	H46	0.087	STO-6G	
C19	0.392	6-31G	H47	0.086	STO-6G	
C20	0.390	6-31G	N48	−0.820	6-31G	
C21	0.473	6-31G	C49	0.570	6-31G	
C22	0.464	6-31G	H50	0.115	STO-6G	
C23	0.378	6-31G	N51	−0.676	6-31G	
C24	−0.073	6-31G	H52	0.208	STO-6G	
C25	−0.099	6-31G	C53	0.192	6-31G	
C26	−0.157	6-31G	H54	0.104	STO-6G	
C27	−0.096	6-31G	C55	0.164	6-31G	
C28	−0.158	6-31G	H56	0.101	STO-6G	

The atomic charges on the peroxynitrite fragment are significantly depended on the environment. The oxygen atom O2 takes part in hydrogen bonds with water molecules and coordinates with iron atom, its charge is less sensitive. The charges of oxygen atoms O1 and O4 in the complex (Figure 2) become closer in values and the charge of nitrogen atom N3 becomes more positive. This also points indirectly to the "isolating" of NO_2 fragment, which is active in the facilitation of rearrangement reaction $[O_2\text{-}NO]^- \rightarrow NO_3^-$ on the active center of hemoglobin in the presence of two water molecules.

Table 5. Some characteristics of peroxynitrite depending on the environment

Compound	Bond lengths			Atomic charges			
	O1O2)	r(O1N3)	r(N3O4)	q(O1)	q(O2)	q(N3)	q(O4)
$[O_2+NO]^-$	1.426Å	1.361Å	1.216Å	0.048	−0.735	0.183	−0.496
$[O_2+NO]^- + 2(H_2O)$	1.473Å	1.356Å	1.204Å	−0.063	−0.804	−0.063	−0.103
$[(H_2O)_2OO\text{-}NO]$ + + Fe-porphyrin + + imidazole	1.469Å	1.339Å	1.212Å	−0.356	−0.758	0.725	−0.579
$[OO\text{-}NO]$ + + Fe-porphyrin + + imidazole	1.463Å	1.462Å	1.174Å	−0.486	−0.780	0.619	−0.341

Consider next the nitrate anion $[NO_3]^-$ which has D_{3h} symmetry in gas phase. The optimal geometry is shown in Figure 3 and structural parameters are compared in the Table 6 in gas phase and in the heme structure. The elongation of chemical bond N3-O2 is noticeable compared with two other bonds (N3-O1 and N3-O4), because the oxygen atom O2 takes part in the formation of coordination bond with iron atom. The oxygen atom O2 also turns out to be the most negatively charged compared with two another and the positive charge of central nitrogen atom N3 becomes noticeably more compared with an isolated nitrate anion $[NO_3]^-$.

30

Table 6. Some characteristics of nitrate anion depending on the environment

Compound	Bond lengths			Atomic charges			
	r(N3O1)	r(N3O2)	r(N3O4)	q(N3)	q(O1)	q(O2)	q(O4)
[NO₃]⁻	1.260Å	1.260Å	1.260Å	0.968	−0.656	−0.656	−0.656
[(H₂O)₂NO₃] + + Fe-porphyrin + + imidazole	1.225Å	1.334Å	1.232Å	1.556	−0.691	−1.053	−0.787
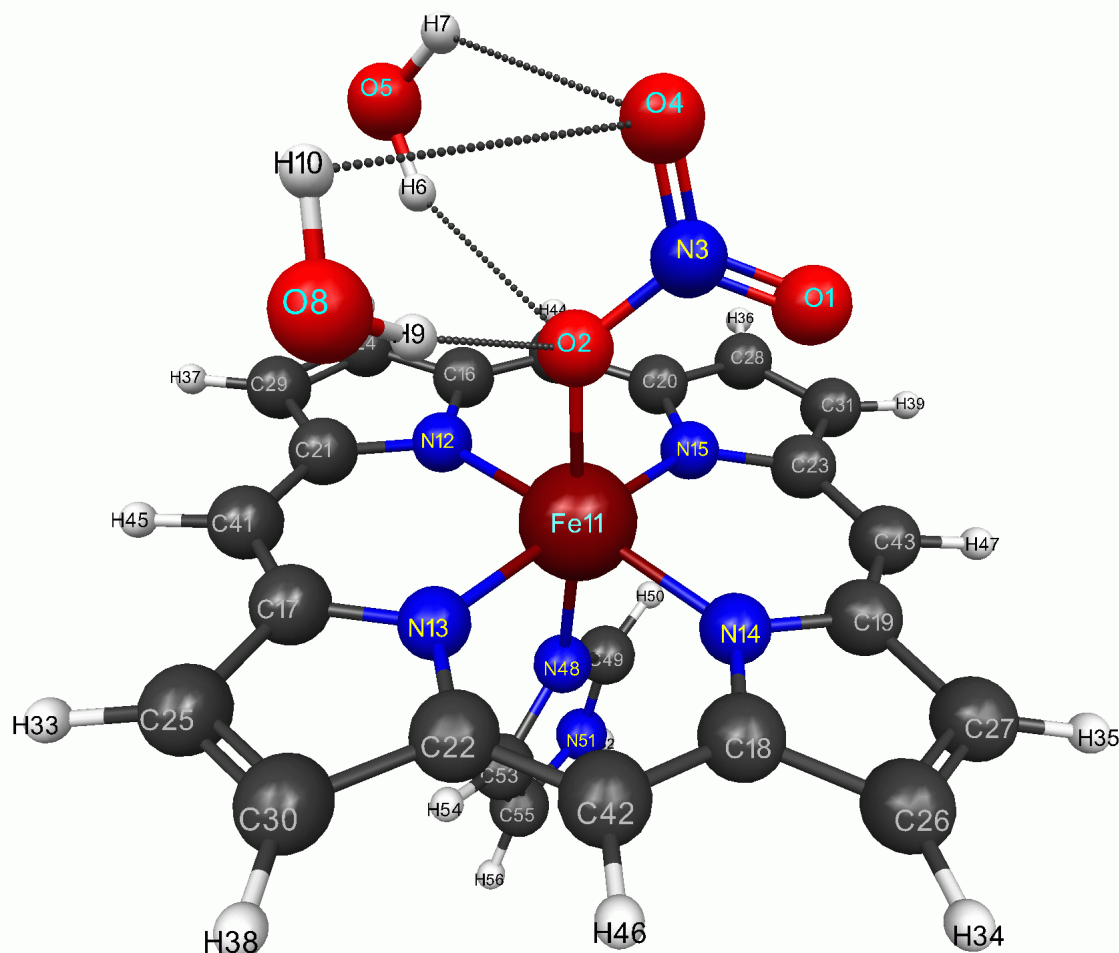
Figure 3. The optimal geometry of complex [(H₂O)₂NO₃] + Fe-porphyrin + imidazole.

On the potential energy surface (PES) corresponding to the total spin $S = 3.5$ there is a local minimum with distance $r(O1N3) \approx 3.5$Å, which may be compared with the local minimum in the "dimeric" structure of peroxynitrite in gas phase on triplet PES [9]. The structure of dimeric complex is shown in the Figure 4. In addition to the unpaired electrons in the 3d-shell of iron atom this complex has unpaired electrons on the radical centers of NO and O_2^- fragment, this is indicated by means of two natural orbitals with occupations close to 1 and localized on these fragments. This complex appears to be characterized by extremely weak bonding energy of NO with O_2^- fragment, this is indicated by rather long distance $r(O1N3) \approx 3.5$Å, which appreciably greater than 3Å with two water molecules (the bonding energy about 2kcal/mol) and greater than 2.9Å in gas phase (the bonding energy about 3.7kcal/mol). The extremely high positive charge of an iron atom attracts our attention in the dimeric complex, it equals +2.9.
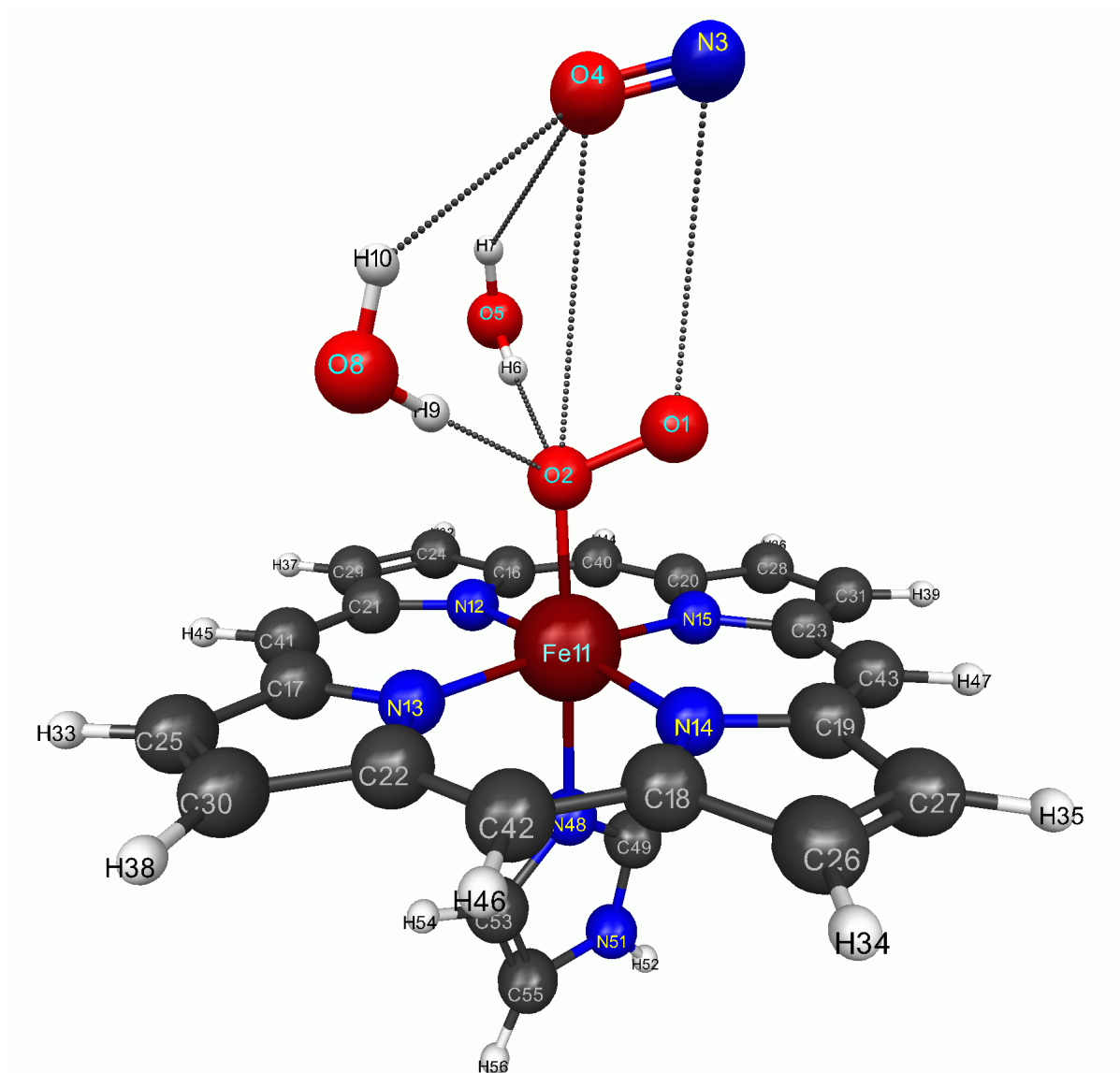
31

Figure 4. The optimal geometry of complex [(H₂O)₂O₂···NO] + Fe-porphyrin + imidazole.

We compare in the Table 7 rearrangement energy of peroxynitrite into the dimer and into the nitrate anion structure. In the first case the rearrangement energy is positive and almost independent on the environment. In the case of nitrate anion it becomes about 20kcal/mol less in absolute value on the active center of hemoglobin.

Table 7. The energy effects of chemical reactions of peroxynitrite

Reaction	Gas phase	With two H_2O	On active center of hemoglobin with two H_2O
$[O_2\text{-}NO]^- \rightarrow O_2^-\cdots NO$	+14.5kcal/mol	+16.8kcal/mol	+16.8kcal/mol
$[O_2\text{-}NO]^- \rightarrow NO_3^-$	−51.0kcal/mol	—	−30.1kcal/mol

Consider next the structure of peroxynitrite complex without the two water molecules; it can arise immediately after formation of chemical bond between O_2 and NO fragments. The structure is represented in the Figure 5 with the geometry parameters given in the last string of Table 5. One can notice the significantly elongated chemical bond r(O1N3) = 1.462Å in comparison with the same bond of 1.339Å in hydrated complex. This denotes from the chemical point of view the substantial weakening of chemical bond between O_2 and NO fragments. The presences of two water molecules stabilize significantly the peroxynitrite

32

fragment, what is necessary for the cleavage of O2-Fe chemical bond before possible ejection of peroxynitrite anion. The hydrotation energy by two water molecules is equal approximately to 16.8kcal/mol; it is twice less than for free peroxynitrite anion: 32.5kcal/mol [9].
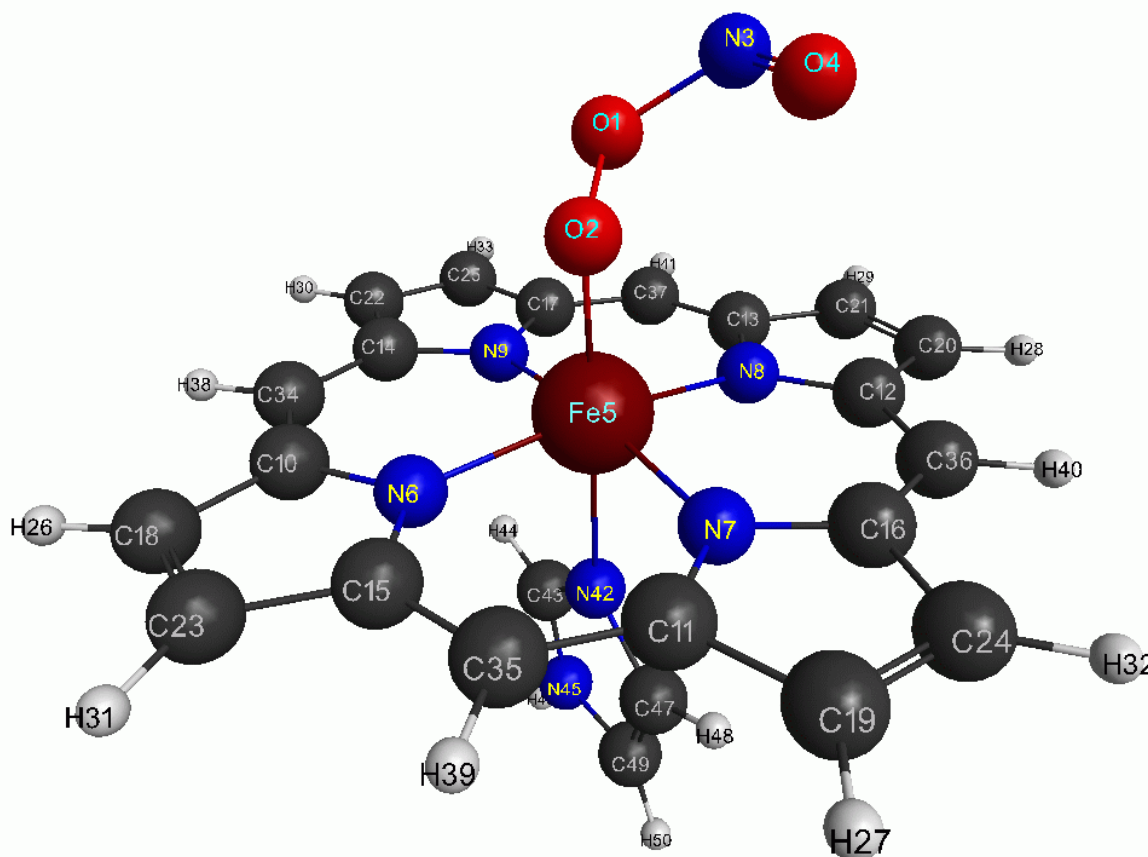

Figure 5. The optimal geometry of complex [OO-NO] + Fe-porphyrin + imidazole.

CONCLUSIONS

The presented results give the structures of anions NO_3^-, $(ONOO)^-$, $(ON\cdots OO)^-$ in the active center of trHbN from *M. tuberculosis* in the MCSCF approach. The *wet* environment is created by two water molecules bounded to the anions and heme.

The tendency of decreasing of regrouping energy is observed in the transformation $(ONOO)^- \rightarrow NO_3^-$ in heme structure compared to that in gas phase. The form of the used wave function is also suitable for the description of bond breaking.

We also suppose that the transformation of *M. tuberculosis* from the latent into an active state can be connected with the other path of elementary chemical reactions in the active center. We have presented the hypothesized role of peroxynitrite structure which can be of interest when some kind of egression path can exist for this anion in hydrophobic protein matrix as it is the case in the detoxification mechanism.

Comprehensive understanding of the biological *M. tuberculosis* role played by trHbN for the survival of *M. tuberculosis* needs an integrated knowledge of protein structure and reaction path when NO radical is approaching to O_2^- ion bound to FeP.

33

APPENDIX 1

Table A1.1. The choice of active space for RASSCF* method

The "lower" subspace		The subspace of full interaction (3d-shell of iron atom)					The "upper" subspace	
89	90	91	92	93	94	95	96	97
$5a_{2u}$	$1a_{1u}$	$15a_{1g}$	$9b_{1g}$	$4e_g$	$4e_g$	$10b_{2g}$	$5e_g$	$5e_g$
ring		$3z^2-r^2$	x^2-y^2	yz	xz	xy	ring	

* The maximum excitation level between subspaces equals 2.

Table A1.2. The characteristics of some lower electronic states in their optimal geometries according to RASSCF method

Term	Total energy, a.u.	Relative energy, eV	Bond lengths Fe-N, Å
$^5A_{1g}$	-2244.254989	0	2.076
$^3A_{2g}$	-2244.210522	1.210	2.033
$^1A_{1g}$	-2244.162560	2.515	2.035
$^1B_{2g}$	-2244.156721	2.674	2.035

Table A1.3. The Mulliken atomic charges in optimal geometry (D_{4h}) of some states according to RASSCF method

Atom*	Basis set	$^5A_{1g}$	$^3A_{2g}$	$^1A_{1g}$	$^1B_{2g}$
Fe1	6-31G*(s,p,d)	1.692	1.669	1.655	1.663
N2–N5	6-31G(d)	-1.296	-1.290	-1.270	-1.287
C6–C13	6-31G	0.545	0.542	0.536	0.542
C14–C21	6-31G	-0.150	-0.147	-0.149	-0.147
H22–H29	STO-6G	0.088	0.088	0.088	0.088
C30–C33	6-31G	-0.179	-0.178	-0.179	-0.178
H34–H37	STO-6G	0.085	0.085	0.085	0.085

* The numeration of atoms according to the Figure 1 in the main text.

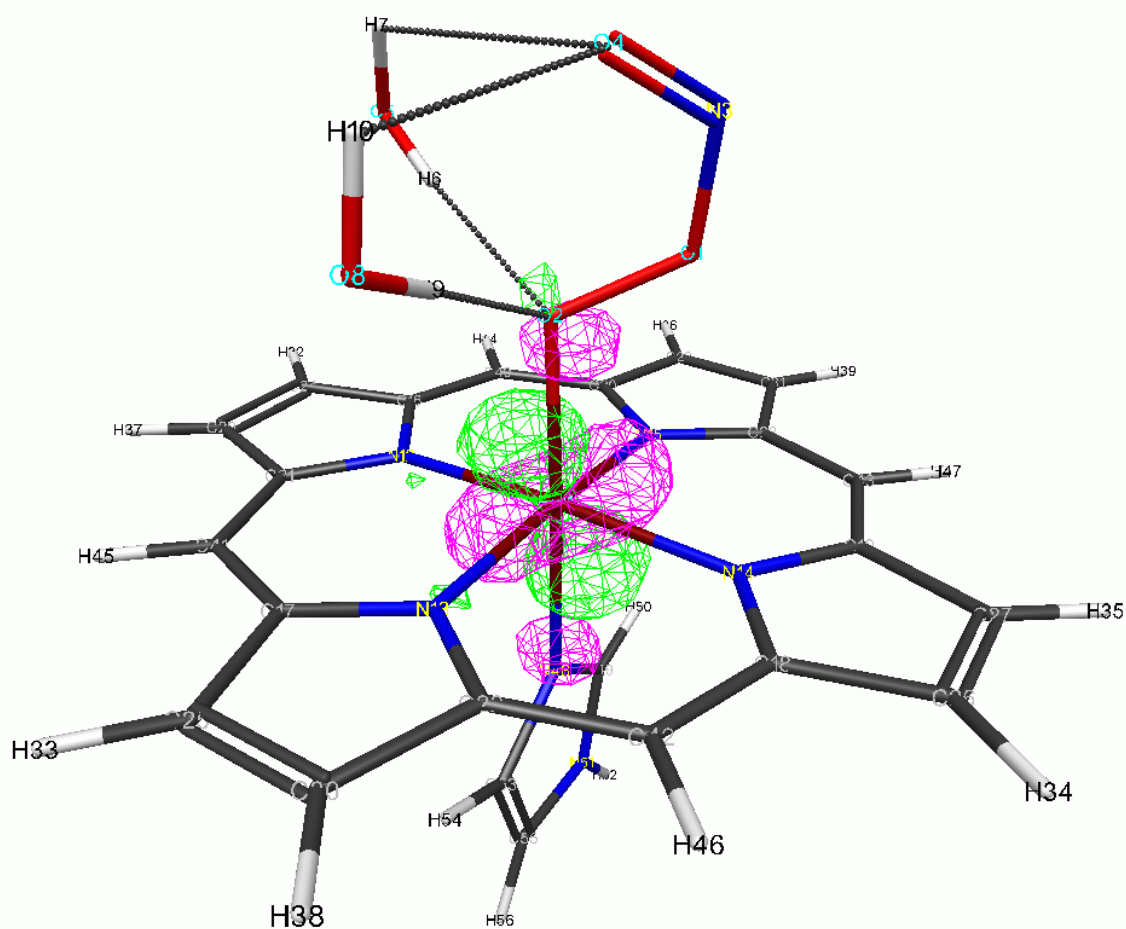# APPENDIX 2.

THE SHAPES OF SOME ACTIVE MOLECULAR ORBITALS

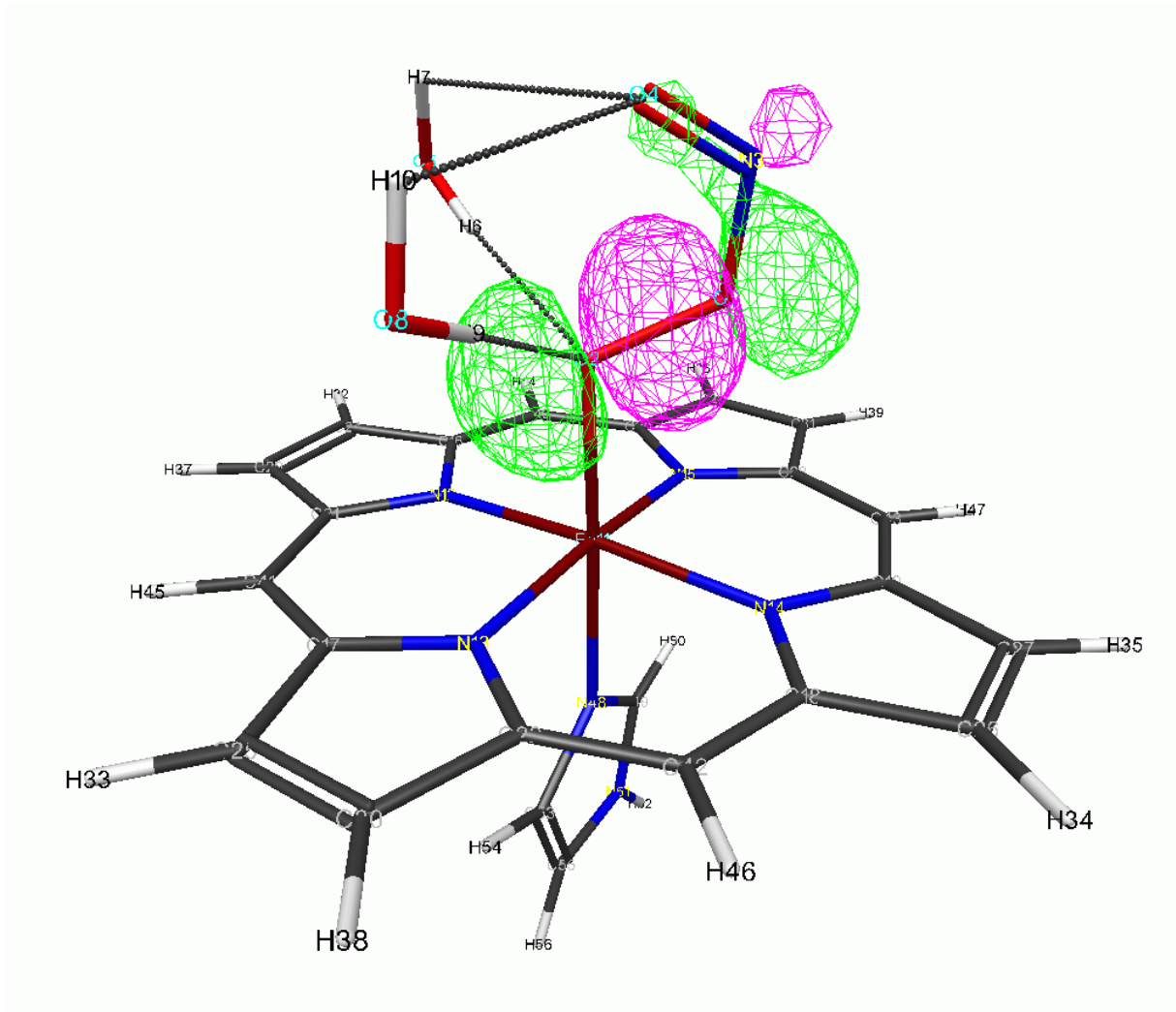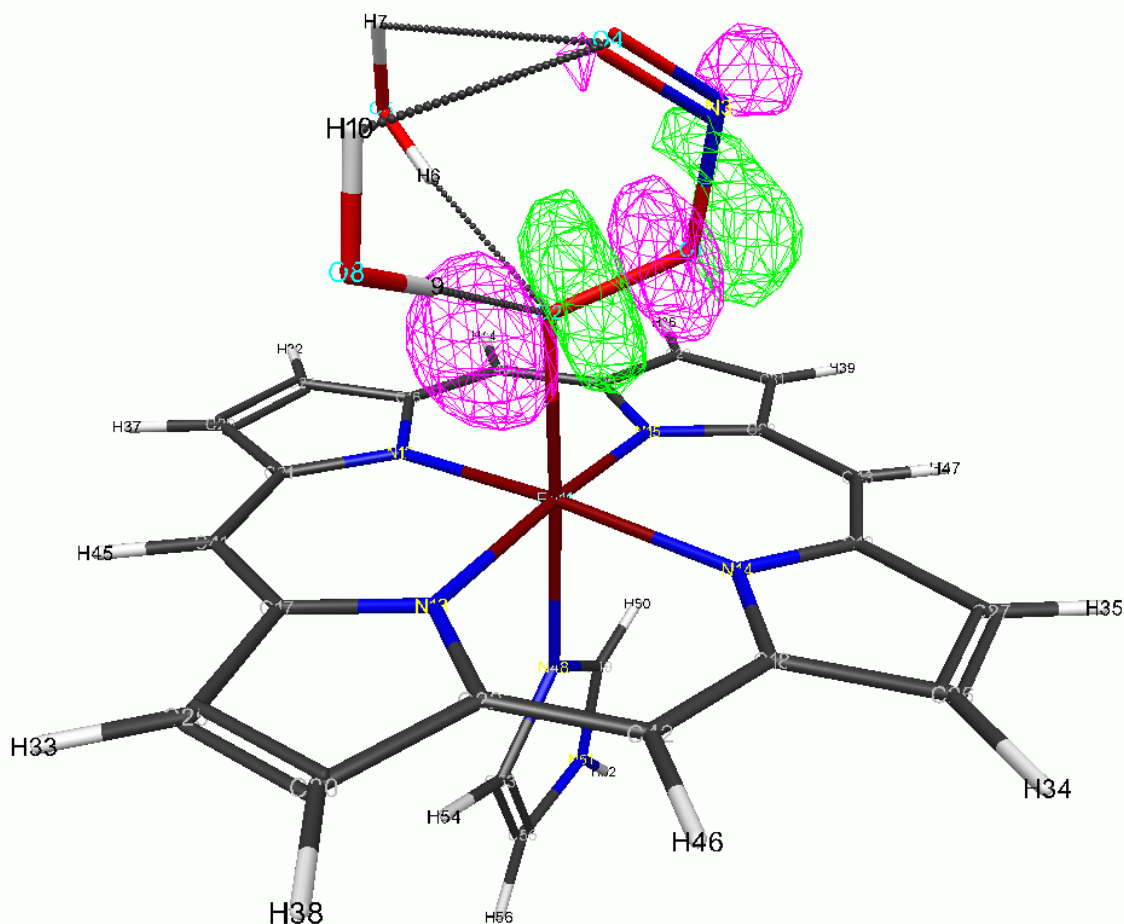**Figure A2.1.** One of the active orbitals from 3d-shell of iron atom.

Figure A2.2. The bonding active orbital σ(O1O2).

Figure A2.3. The antibonding active orbital σ*(O1O2).

REFERENCES

1. Milani M., Pesce A., Quellet Y. et all. *EMBO Journal.* 2001. V. 20. № 15. P. 3902–3909.
2. Milani M., Pesce A., Quellet Y. et all. *Journal Biological Chemistry*. 2004. V. 279. № 20. P. 21520–21525.
3. *The porphyrin Handbook.* Eds. Kadish K. M., Smith K. M., Guilard R. Academic Press, 2000. V. 7: Theoretical and Physical Characterisation. 423p.
4. Marti M. A., Bidon-Chanal A, Crespo A. et al. *J. Am. Chem. Soc.* 2008. V. 130. P. 1688–1693.
5. Bidon-Chanal A., Marti M. A., Estrin D. A., Luque F. J. In: *Self-Organization of Molecular Systems.* Eds. Nino Russo, Antonchenko V. Ya., Kryachko E. NATO Science for Peace and Security, Series-A. Springer, 2009. P. 33–48.
6. Tsai H., Hamilton T. P., Tsai J. M., van der Woerd M., Harrison J. G., Jablonsky M. J., Beckman J. S., Koppenol W. J. *J. Phys. Chem.* 1996. V. 100. P. 15087–15095.
7. Harkless J. A. W., Rodriguez J. H., Lester Jr. W. A. *Jour. Chem. Phys.* 2003. V. 118. № 11. P. 4887–4992.
8. Lebrero M. C. G, Perissinotti L. L., Estrin D. A. *J. Phys. Chem. A.* 2005. V. 109. P. 9598–9604.
9. Simon K. V., Tulub A. V. *Optics and Spectroscopy.* 2009. V. 107. № 1. P. 46–53.

10. Formey D, Thompson W. E., Jacox M. E. *J. Chem. Phys.* 1993. V. 99. № 10. P. 7393–7403.
11. Stanton J. *J. Chem. Phys.* 2007. V. 126. P. 134309–134314.
12. Poli R., Harvey J. N. *Chem. Soc. Rev.* 2003. V. 32. P. 1–8.
13. Pau M. Y. M., Lipscomb J. D., Solomon E. I. *PNAS.* 2007. V. 104. № 47. P. 18355–18362.
14. Bikiel D. E., Boechi L., Capece L., Crespo A. et all. *Phys. Chem. Chem. Phys.* 2006. V. 8. P. 5611–5628.
15. Schmidt M. W., Baldridge K. K., Boatz J. A., Elbert S. T., Gordon M. S., Jensen J. H., Koseki S., Matsunaga N., Nguyen K. A., Su S. J., Windus T. L., Dupuis M., Montgomery J. A. *J. Comput. Chem.* 1993. V. 14. P. 1347–1363.
16. Panin A. I., Simon K. V. *International Journal of Quantum Chemistry.* 1996. V. 59. P. 471-475.
17. Nakano H. *J. Chem. Phys.* 1993. V. 99. P. 7983–7992.
18. Piecuch P., Wloch M. *J. Chem. Phys.* 2005. V. 123. P. 224105-1–224105-10.
19. Wloch M, Gour J. R., Piecuch P. *J. Phys. Chem. A.* 2007. V. 111. P. 11359–11382.
20. Bode B. M. and Gordon M. S. *J. Mol. Graphics and Modeling*. 1998. V. 16. P. 133-138.
21. Ivanic J. *J. Chem. Phys.* 2003. V. 119. № 18, P. 9364-9376.